CHEMISTRY
A EUROPEAN JOURNAL

DOI: 10.1002/chem.201101940

Switchable Self-Assembly of a Bioinspired Alkyl Catechol at a Solid/Liquid Interface: Competitive Interfacial, Noncovalent, and Solvent Interactions

Javier Saiz-Poseu,[a, b] Jordi Faraudo,[c] Antoni Figueras,[d] Ramon Alibes,[d] Felix Busqué,*[d] and Daniel Ruiz-Molina*[a]

Abstract: The large tendency of catechol rings to adsorb on surfaces has been studied by STM experiments with molecular resolution combined with molecular-dynamics simulations. The strong adhesion is due to interactions with the surface and solvent effects. Moreover, the thermodynamic control over the differential adsorption of **1** and the nonanoic solvent molecules has been used to induce a new temperature-induced switchable interconversion. Two different phases that differ in their crystal packing and the presence of solvent molecules coexist upon an increase or decrease in the temperature. These results open new insight into the behavior of catechol molecules on surfaces and 2D molecular supra-structures.

Keywords: catechol · molecular dynamics · self-assembly · scanning tunneling microscopy · switchable materials

Introduction

Catechols are benzene derivatives that contain two neighboring hydroxy groups in the aromatic ring. This apparently simple structure can be found in Nature taking part in several very different processes. One of the most well-known examples of such versatility is the aminoacid L-3,4-dihydroxyphenylalanine (DOPA), which plays a crucial role in the strong adhesive capacity of mussels.[1] Indeed, recent evidence suggests that mussels and other marine organisms secrete protein-based materials containing this amino acid. Oxidation leads to intermolecular cross-linking of the plaque proteins[2] with interfacial adhesion capacities thanks to chemical interactions between the catechol form of DOPA and surface functional groups of a large variety of substrates (e.g., minerals, metal surfaces, and wood among others).[1] Alkyl catechols are also the principal ingredients and responsible for the coating capacities of ancient Asian lacquers,[3] such as urushiol, laccol, and thitsiol.[4] All these saps present catechol compounds with alkyl and alkenyl chains of different length, degree of saturation, and position in the benzene ring. The polymerization of these compounds through the enzymes (laccases) that are contained in their own sap leads to the formation of a cross-linked polymer that constitutes the protective film thanks to its tendency to adsorb on surfaces.[5]

This ability of catechol derivatives to interact with surfaces has been exploited by many scientists worldwide to develop new functional adhesives[6] and protective-coating films.[7] However, despite numerous successfully developed and applied studies so far, understanding the basic behavior of catechols on surfaces still remains a challenge. These studies should yield basic information about their assembly and interaction on the nanoscale and are of vital relevance for the development of new materials with improved properties.

Scanning tunneling microscopy (STM) is an excellent technique for such studies.[8] Thanks to its intrinsic molecular resolution, STM can allow the direct observation, and therefore, the direct study and modelization of molecule/molecule and molecule/surface interactions.[8a,c–e,i,k,m–q] Although, scarce examples of catechols on surfaces have been studied by STM[9] so far, none of these examples are at the liquid/solid interface to simulate a real situation.[10]

To fill this gap, alkyl catechol **1** has been successfully studied by STM in this investigation at different temperatures in the presence of solvent. The resulting self-assembly motives

[a] J. Saiz-Poseu, Dr. D. Ruiz-Molina
Centro de Investigación en Nanociencia y Nanotecnología (ICN-CSIC)
Esfera UAB, Edificio CM7, Campus UAB, 08193
Cerdanyola del Vallès, Barcelona (Spain)
Fax: (+34) 935813717
E-mail: druiz@cin2.es

[b] J. Saiz-Poseu
Fundación Privada ASCAMM
Unidad de Nanotecnología (NANOMM)
Parc Tecnològic del Vallès, Av. Universitat Autònoma, 23-08290
Cerdanyola del Vallès, Barcelona (Spain)

[c] Dr. J. Faraudo
Institut de Ciència de Materials de Barcelona (ICMAB-CSIC)
Campus de la UAB, 08193
Cerdanyola del Vallès, Barcelona (Spain)

[d] A. Figueras, Dr. R. Alibes, Dr. F. Busqué
Department de Química, Universitat Autònoma de Barcelona
Edifici C, Campus UAB, 08193
Cerdanyola del Vallès, Barcelona (Spain)
E-mail: felix.busque@uab.es

Supporting information for this article is available on the WWW under http://dx.doi.org/10.1002/chem.201101940.

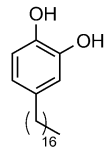

1

have been rationalized according to theoretical calculations that yield important information about the different parameters that govern the assembly of catechols on surfaces. Moreover, the knowledge gained has been used to promote a 2D temperature-induced switchable molecular self-assembly, an area of great research interest nowadays within molecular nanotechnology.

Results and Discussion

Synthesis: Prior to this study, two different synthetic procedures have already been reported for **1**.[11] However, neither of them allowed us to obtain **1** in the high-purity standards required for STM experiments. Therefore, it was necessary to develop the new synthetic methodology outlined in Scheme 1 for the preparation of **1** in multigram quantities and with the required purity.

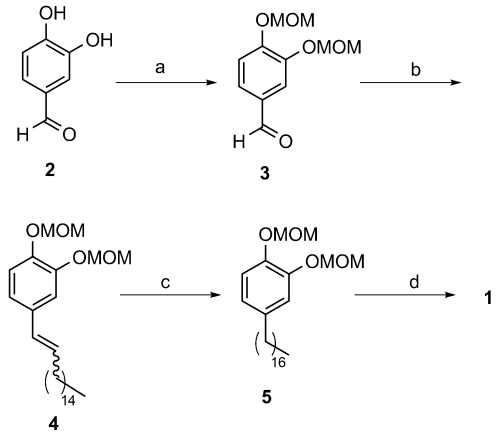

Scheme 1. Synthesis of catechol **1**. a) Methoxymethyl bromide, iPr$_2$EtN, DMAP, CH_2Cl_2 (99%); b) 1-hexadecyltriphenylphosphonium bromide, tBuOK, THF (70%); c) H_2, Pd/C, ethyl acetate (98%); d) HCl (cat.), MeOH (86%). DMAP = 4-dimethylaminopyridine, MOM = methoxymethyl ether.

Our synthesis started from commercially available 3,4-dihydroxybenzaldehyde (**2**), which was converted into the methoxymethyl(MOM)-protected derivative **3** under standard conditions in almost quantitative yield. Next, the Wittig reaction of aldehyde **3** with hexadecyltriphenylphosphonium bromide and potassium *tert*-butoxide in dry THF afforded the olefin **4** in 70% yield as a 9:1 mixture of the *Z* and *E* isomers. The use of other bases, such as *n*BuLi, proved to be less efficient for this transformation. Conventional hydrogenation of alkene **4** under palladium catalysis gave **5** in 98% yield. Finally, cleavage of the MOM ethers in methanol heated to reflux under acidic catalysis provided the target 4-alkylcatechol **1** in 86% yield.

STM and self-assembly studies: A drop of a nonanoic solution of **1** (2 mg mL^{-1}) at room temperature was cast onto a freshly cleaved highly oriented pyrolytic graphite (HOPG) surface. The experimental conditions described in Figure 1

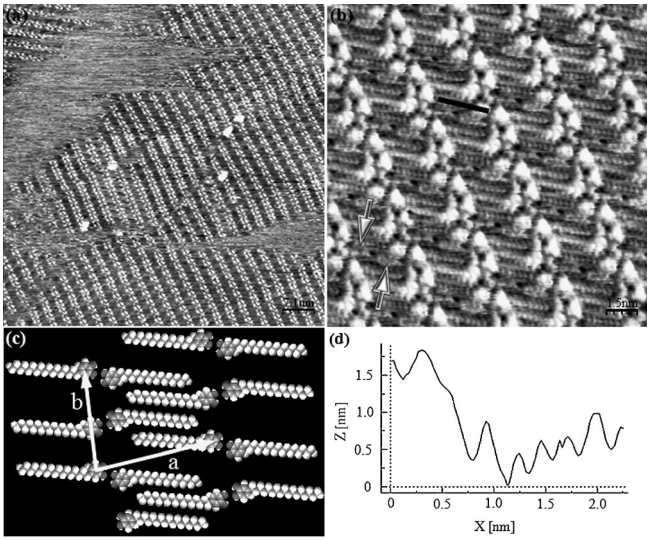

Figure 1. Self-assembly patterns obtained with **1** at the nonanoic acid/HOPG interface. a) Large domains of the α phase are observed (scanning conditions: 71 × 71 nm, I_{set} = 30 pA, V_{bias} = 350 mV). b) Zoom area of the α phase. The arrows point at the hollows where nonanoic acid is coadsorbed within the pattern of **1** (scanning conditions: 15 × 15 nm, I_{set} = 25 pA, V_{bias} = 400 mV). c) Tentative molecular model for the arrangement of **1** within the α phase (unit-cell parameters: $a = (3.0 \pm 0.2)$, $b = (2.8 \pm 0.2)$ nm; $\gamma = (82 \pm 3)°$). d) Profile marked in (b), which is coincident with the length of a molecule of **1**.

were used to obtain stable and reproducible images at least over three independent surface areas. In all the cases, molecular arrays with domains (the so-called α phase) that extend from 10 nm up to a few hundred nanometers are observed. Moreover, the resulting molecular packing was obtained with high reproducibility between different casting experiments of freshly prepared samples and its stability was assessed by taking STM images at different time intervals. The analysis of the images (Figure 1a and b) shows that the high-contrast aromatic cores form rows, with shaded lines, which correspond to the long alkyl chains, interdigitating between them. Moreover, two different alternating orientations of the heads with respect to the alkyl chains can be distinguished. A molecular model that justifies such organization is schematized in Figure 1c.

Four molecules of **1** are perfectly packed following the disposition previously described. The profile marked in Figure 1d for one of them is coincident with the expected length of 2.1 nm. Within the interdigitated alkyl chains, the appearance of darker gaps that break the periodicity of the pattern approximately every 1.8 nm can be observed. Such distance is in good agreement with the distance that represents approximately four neighboring alkyl chains observed in the experimental image (marked with an arrow in Fig-

ure 1b). By taking into account the calculated unit cell area of 8.2 nm^2 and the number of molecules of **1** per unit cell (i.e., 4), a free surface of approximately 1.3 nm^2 is expected to remain unoccupied. This surface area represents enough space for the accommodation of two nonanoic acid molecules per unit cell (not represented for the sake of simplicity), in good accord with the match between the gap dimensions and those of the nonanoic acid. Therefore, the α phase is most likely a coadsorption pattern between **1** and solvent molecules, as already described for other molecular arrays on surfaces.[12]

A regular modulation in the image contrast is also observed most likely due to the influence of the underlying substrate, which shows a tendency to form Moiré patterns.

By taking into account the fact that nonanoic acid molecules, that is, the dominant species within the droplet, also exhibit a considerable tendency to be adsorbed (see Figure S1 in the Supporting Information), the ability to adsorb on the surface between **1** and the noanoic acid is the first indication of the large tendency of alkyl catechols to remain on the surface. However, it must be also emphasized that an increase in the concentration of **1** in the deposited droplet is not enough to completely displace nonanoic acid molecules from the molecular arrays, thus leading once more to the formation of domains formed by the α phase, at least under the concentration range studied.

Molecular dynamics (MD) simulations: The thermodynamics for **1** and nonanoic molecules to be transferred from the solution to a graphite surface were studied by performing MD simulations combined with adaptive biased force (MD-ABF) calculations. Full details of the procedures and algorithms are given in the Experimental section. The simulated system consists of a liquid solution composed of 14 molecules of **1** and 400 nonanoic acid molecules. This molecular ratio corresponds to an approximate concentration of 2 $mg\,mL^{-1}$, typical of the experimental conditions used. First, the bulk solution was equilibrated by performing MD simulations at 20 °C and 1 atmosphere. The solution was placed in contact with a graphite surface of 32.65 nm^2, which was immediately covered by molecules (i.e., nonanoic acid and **1**). A second set of MD simulations were run to allow further equilibration and adsorption/desorption events at the surface. Afterwards, MD-ABF simulations were performed on the resulting system to obtain the thermodynamic free energy associated with the transfer of catechol and nonanoic acid molecules from the liquid to the graphite surface as a function of the distance. The results for the free-energy profile are shown in Figure 2, and representative snapshots of the transfer of molecules from the surfaces to the liquid solution are shown in Figure 3.

The adsorption minimum corresponds to a gain in free energy of 122 $kcal\,mol^{-1}$ for **1** and 45 $kcal\,mol^{-1}$ for the nonanoic acid (Figure 2). These results demonstrate that even though nonanoic acid is predominant, the larger affinity of **1** for the surface can perfectly result in the coadsorption of both compounds on the α phase. The higher affinity of alkyl

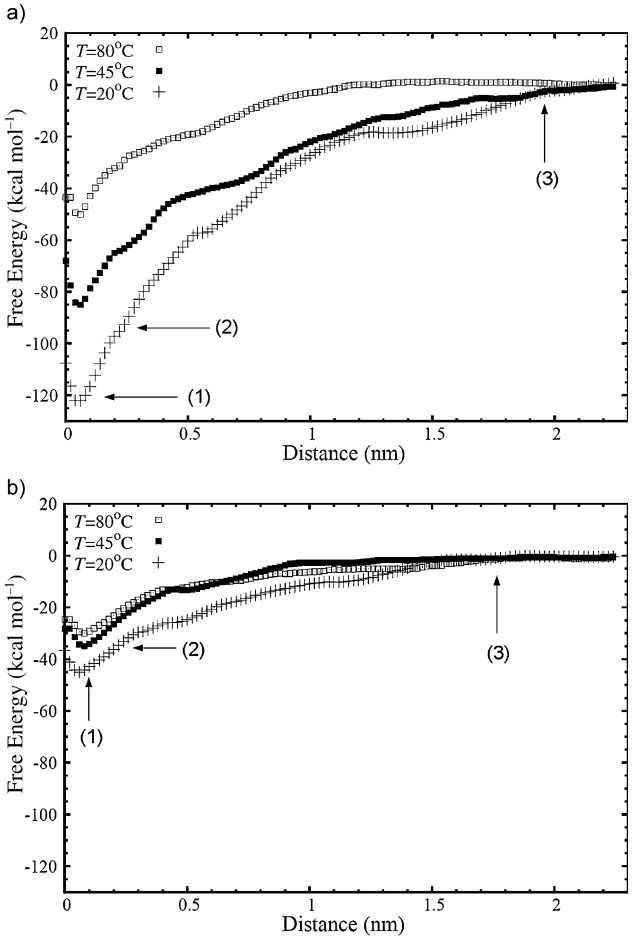

Figure 2. Top) Free-energy for the transfer of a 4-heptadecylcatechol molecule (a) and a nonanoic acid molecule (b) from the bulk solution to the graphite surface as a function of the distance z of the center of mass of the molecule to the surface. The MD-ABF calculations were performed at 20, 45, and 80 °C.

catechols for the surface is not only due to its longer alkyl chain but also to interactions that originate at the head group, which can be seen in the snapshots shown in Figure 2a. These images show three different steps from MD-ABF simulations in which an adsorbed molecule of **1** is removed from the graphite surface to the liquid solution. Interestingly, in the desorption process, the alkyl chain is detached first, whereas the head group still remains on the surface and maintains contact with the graphite, probably through π–π interactions and hydrogen bonds with other head groups. On the contrary, the snapshots in Figure 3b show that the nonanoic acid molecules detach from the surface without showing any specific affinity of the carboxylic group for the surface. The high affinity of the head group of **1** for the surface is also favored by thermodynamic factors, which was confirmed by comparing the results in Figure 2 with the interaction energy obtained by molecular/mechanics calculations between a single isolated molecule (without solvent) and the surface. In this case, a gain in energy of only 47.3 $kcal\,mol^{-1}$ was obtained for transferring a single

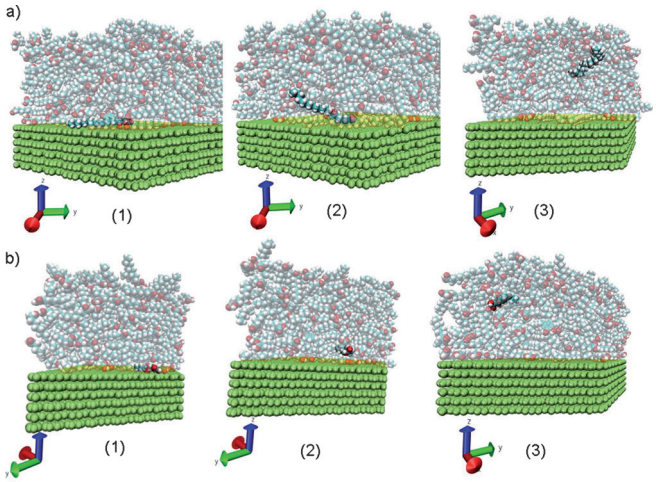

Figure 3. Snapshots of three different steps in the MD-ABF simulation for the transfer of a molecule from adsorption at the graphite surface to bulk solution as a function of the distance z of the center of mass of the molecule to the surface. These images correspond to particular configurations that contribute to the free-energy profiles at the locations marked by arrows in Figure 2. The transferred molecule is emphasized and all the other molecules of the system are shown as translucent. The picture was made by using the VMD software.[1] a) Transfer of a molecule of **1**; b) transfer of a nonanoic acid molecule.

molecule of **1** from an infinite distance onto the graphite surface. Therefore, the direct surface/molecule interaction energy represents only 38% of the free-energy gain obtained in transferring an alkyl catechol molecule from bulk solution at 20°C onto the surface. In the case of nonanoic acid, a gain in energy of 24.3 kcal mol^{-1} for the direct molecule/surface interaction was obtained, which represents 54% of the free energy of adsorption (45 kcal mol^{-1}) at 20°C.

This comparison shows that the high affinity of the alkyl catechol molecule is of thermodynamic origin, instead of a purely energetic preference. If this possibility is true, the system should exhibit a strong dependence on the temperature, which was confirmed by performing additional MD-ABF calculations at 45 and 80°C. The resulting free energies of adsorption at such temperatures are also shown in Figure 2. In the case of **1**, the free-energy gain decreases from 122 kcal mol^{-1} at 20°C to 85 and 50 kcal mol^{-1} at 45 and 80°C respectively. Interestingly, the effect of temperature is much more pronounced for **1** than for the nonanoic acid, for which a decrease from only 45 kcal mol^{-1} at 20°C to 35 and 30 kcal mol^{-1} at 45 and 80°C, respectively, was obtained. According to these results, it would be likely to expect a differential adsorption/desorption behavior of both compounds with temperature, therefore, with implications for the self-assembly patterns observed in the STM experiments.

Variable-temperature STM experiments: A drop of a nonanoic acid solution of **1** (2 mg mL^{-1}) was cast onto a freshly cleaved HOPG surface at room temperature. Initially, the α phase covers most of the surface, although an increase in the temperature up to 45°C induces the loss of the molecular domains, which is most likely due to the considerable thermal drift.[13] When the system is allowed to cool to room temperature, large and stable domains of a new phase (the so-called the β phase) were observed over different areas of the substrate, thus replacing the initial α phase. The new molecular packing is not a transient phase that is obtained with high reproducibility over different experiments, and the stability of this phase was assessed by taking different STM images over the same region at different time intervals. A representative image of the new β phase is shown in Figure 4.

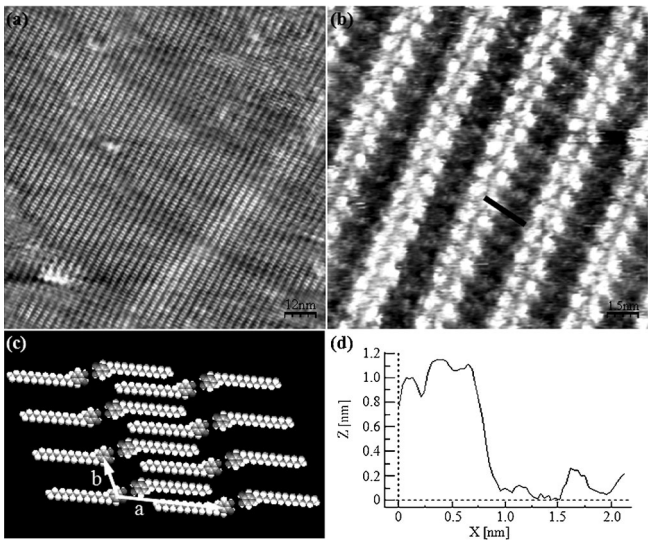

Figure 4. Self-assembly pattern of **1** at the nonanoic acid/HOPG interface. a) Large domains of the resulting β phase upon annealing at 45°C (scanning conditions: 125×125 nm, I_{set}=40 pA, V_{bias}=400 mV). b) Detail of one of the domains in which no coadsorbed solvent molecules can be distinguished (scanning conditions: 15×15 nm, I_{set}=40 pA, V_{bias}=300 mV). c) Tentative molecular packing for **1** within the β phase (unit-cell parameters: $a=(3.1\pm0.1)$, $b=(1.1\pm0.1)$ nm; $\gamma=(105\pm2)°$). d) Profile marked in (b), which is coincident with the length of a molecule of **1**.

The molecular packing of this new phase also shows that the high-contrast aromatic cores are arranged in rows of dimers with interpenetrated alkyl chains between them. However, the images are poorly resolved relative to the resolution obtained for the α phase. Although several experiments were tried, the resolution did not improve, which is not entirely explainable by the smaller lattice constants, at least for the resolution of the alkyl chains. However, poor resolution was likely due to tip defects and/or the influence of the substrate and packing of the alkyl chain. A model that shows the tentative packing of the β phase is shown in Figure 4c. There are two main differences with respect to the α phase: 1) All the dimers are oriented in the same direction (whereas two different alternating orientations of the heads with respect to the alkyl substituents are observed in the α phase) and 2) denser packing of the alkyl chains results due to the lack of solvent molecules. This higher density is reflected in the unit cell with an area of only 3.5 nm^2,

which is occupied by two molecules of **1**. The resulting free area of only 0.02 nm^2 is not enough to fit the nonanoic acid molecules.

A further increase in the temperature to 80 °C induces the loss of the molecular domains most likely due, once more, to considerable thermal drift. Surprisingly, when the system is allowed to cool to room temperature, large and stable domains of the α phase are recovered again. No signal of the β phase can be observed over different scanned areas of the substrate.

This fact allowed us to establish temperature-induced switching between both phases (Figure 5). It is important to emphasize that the temperature-induced interconversion between the different phases is completely reversible over several different cycles; therefore, one of the two phases can be achieved by simply controlling the temperature.

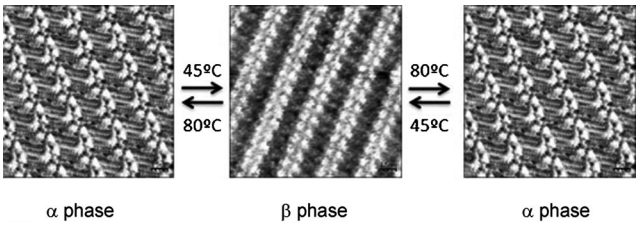

Figure 5. Schematic representation of the temperature-induced switching between the α and β phases. The images were obtained after heating to the temperature indicated and allowing the system to cool to room temperature in each case.

To gain greater insight into this differential temperature behavior, the formation energies for both phases were calculated from the free-energy data shown in Figure 2. In the case of the α phase, the unit cell of 8.2 nm^2 has four molecules of **1** and two nonanoic acid molecules. Therefore, the free energy gain at 20 °C is $(4\times122+2\times45)/8.2\approx70.5$ kcal mol^{-1} for each nm^2 unit of the surface. For the β phase, there is a unit cell of 3.5 nm^2 containing two molecules of **1**. Hence, the free-energy gain from the transfer of molecules from the solution to the surface is $(2/3.5)\times122\approx69.7$ kcal mol^{-1} for each nm^2 unit of the surface covered. Interestingly, the free-energy gain is slightly favored for the α phase, which justifies its preferential thermodynamic formation. However, the difference at 20 °C for both phases is quite small, which would explain that in some cases it is possible to experimentally observe their coexistence (see Figure S2 in the Supporting Information) or why MD calculations could not isolate one of the two phases (see Figure S3 in the Supporting Information).

Upon formation of the α phase at 20 °C, an increase of the temperature to 80 °C is enough to induce the desorption of both nonanoic acid and **1**. Then, the mechanism for the formation at 80 °C is similar to that at 20 °C because both families of molecules are desorbed from the surface before the formation of the corresponding phase. Under these premises, it is also possible to calculate the formation energy at 80 °C from the free-energy data shown in Figure 2. The estimated formation energies per nm^2 unit of the surface are $(4\times50+2\times30)/8.2\approx31.7$ and $(2/3.5)\times50\approx28.6$ kcal mol^{-1} for the α and β phases, respectively. This outcome means that the formation of the α phase is even more favored at higher temperatures, as expected for a thermodynamically controlled mechanism.

Therefore, why is this simple energy estimation, which justifies the formation of the α phase at 20 and 80 °C, not valid at 45 °C at which the β phase is obtained instead? A tentative mechanism that may explain such divergence is shown in Figure 6. Upon formation of the α phase at 20 °C, an increase of the temperature to 45 °C is enough to displace the nonanoic acid molecules but not to displace the adsorption equilibrium for **1**, which remains on the surface due to its higher affinity. The desorption of nonanoic molecules leads to voids with a free area of 1.44 nm^2 per unit cell, thus resulting in a quite unstable structure. This situation forces **1** to reorganize and fill the empty spaces, thus resulting in the formation of the more compact β phase. This behavior means that the formation energy to be considered is required exclusively for reorganization but is not required to bring molecules from solution.

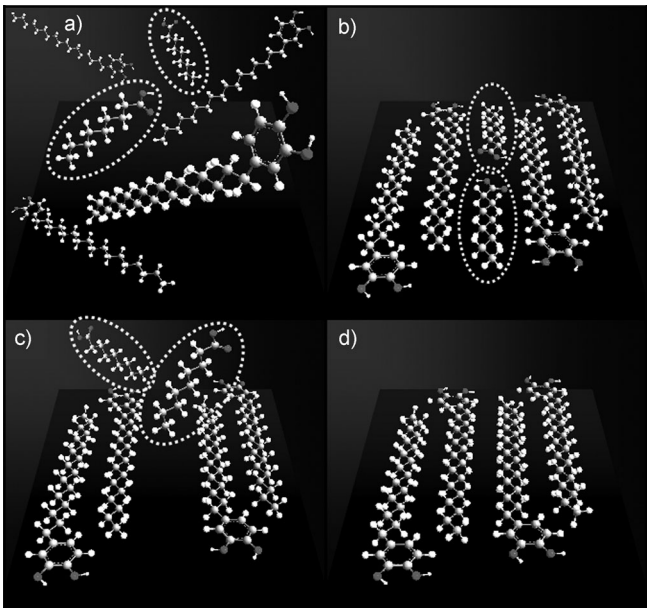

Figure 6. A 3D representation of the tentative mechanism proposed for the transition from the α to β phase. a) Molecules in solution; b) arrangement of the molecules in the α-phase unit cell; c) the coadsorbed solvent molecules are desorbed from the surface during annealing to leave voids in the monolayer; d) the 4-heptadecylcatechol molecules rearrange to fulfill the free room, thus giving rise to the β phase.

Conclusion

Compound **1** has been shown to exhibit a large tendency to adsorb on surfaces, as confirmed by combined STM experiments and MD simulations. A gain in free energy of

122 kcal mol^{-1} for **1** has been calculated, being considerably larger than that found for nonanoic acid (45 kcal mol^{-1}). Such an anomalously high gain is the result of the high affinity of **1** for the surface (purely energetic preference) but is mainly because of solvent effects (thermodynamic origin). In the present case, such thermodynamic effects are nicely exemplified by the relatively poorly solvation of **1** in nonanoic acid. The structure of the nonanoic acid, liquid at room temperature and over, is highly disrupted by the structurally different catechol moieties. Once on the surface, the strongest interaction energy of **1** with HOPG can be associated Van der Waals interactions with the alkyl chains and hydrogen-bonding interactions between the catechol moieties. In fact, our MD-ABF simulations show that the desorption of **1** from the surface proceeds first through the alkyl group, whereas the catechol moiety tends to remain in contact with the surface. These results yield important information about the relevance of entropic factors, such as solvent and environment effects, on the self-assembly of molecular materials on surfaces. In accord with their thermodynamic origin, the adsorption pattern of **1** exhibits strong temperature dependence. This fact has been used to establish a switchable interconversion between two different phases of **1** with different molecular packing on the surface, simply by increasing or decreasing the temperature over several cycles. This result opens the door to the development of new temperature-induced switchable supramolecular structures on surfaces.

Finally, important information has also been obtained about the correct implementation of MD. One may wonder whether total-energy calculations obtained by using simple molecular mechanics can be enough to characterize the interaction of molecules with surfaces as this approach is usually carried out in many studies that analyze STM results. However, the thermodynamic MD-ABF calculations reported in this study involve, from a computational point of view, very expensive simulations because our simulations include not only the surface and adsorbed molecules but a large number of solvent and solute molecules to model the solution in contact with the surface. We have shown that, at least in our example, such expensive calculations including thermodynamic parameters are not only required but are essential for a proper interpretation of the results. Also, we cannot discard important effects such as the dynamic exchange of individual molecules and dynamic effects at domain boundaries, which may have a critical influence on the interpretation of the structure of the observed structures.

Experimental Section

General experimental procedures and spectrophotometers data are included in the Supporting Information.

3,4-Bis(methoxymethoxy)benzaldehyde (3):[14] *i*Pr$_2$EtN (7.6 mL, 43.2 mmol) and DMAP (0.10 g) were added to a stirred solution of 3,4-dihydroxybenzaldehyde (1.0 g, 7.2 mmol) in CH_2Cl_2 (10 mL) at 0 °C. Methoxymethyl bromide (2.6 mL, 28.8 mmol) was added dropwise to the reaction mixture with the temperature kept at 0 °C for 1 h. Afterward, the reaction mixture was allowed to reach room temperature and heated to reflux overnight. The reaction mixture was allowed to cool to room temperature and washed with brine (15 mL). The phases were separated and the aqueous layer was extracted with $CHCl_3$ (3×7 mL). The combined organic layers were dried over $MgSO_4$, and concentrated under reduced pressure to yield an oil, which was purified by column chromatography on silica gel with hexanes/EtOAc (10:1) as the eluent to give **3** as a slightly yellow oil (1.62 g, 99% yield).

(*Z*)-/(*E*)-1,2-Bis(methoxymethoxy)-4-(heptadec-1-enyl)benzene (4): Hexadecyltriphenylphosphonium bromide (4.10 g, 7.29 mmol) was dissolved in anhydrous THF (40 mL) under nitrogen and *t*BuOK (1.33 g, 12.6 mmol) was added portionwise. After stirring for 45 min, a solution of **3** (1.5 g, 6.63 mmol) in anhydrous THF (10 mL) was added to the reaction mixture, which was stirred for a further 3 h. The reaction was quenched with water (30 mL), the phases were separated, and the aqueous layer was extracted with EtOAc (3×10 mL). The combined organic phases were dried over $MgSO_4$ and concentrated under vacuum to afford an oil, which was purified by column chromatography on silica gel with hexanes/EtOAc (20:1) as the eluent to give a mixture of (*Z*)-**4** and (*E*)-**4** (≈9:1) as a slightly yellow oil (1.97 g, 70% yield). Repeated column chromatography allowed isolation of the pure isomers. (*Z*)-**4**: ^{1}H NMR (250 MHz, $CDCl_3$): δ=7.15 (d, J=2 Hz, 1H), 7.10 (d, J=7.1 Hz, 1H), 6.89 (dd, J=7.1 Hz, J=2 Hz, 1H), 6.32 (d, J=11.6 Hz, 1H), 5.60 (dt, J=11.6, 7.1 Hz, 1H), 5.20 (s, 4H), 3.50 (s, 6H), 2.32 (m, 2H), 1.45 (m, 2H), 1.40–1.20 (m, 24H), 0.88 ppm (t, J=6.3 Hz, 3H); ^{13}C NMR (62.5 MHz, $CDCl_3$): δ=146.6, 145.6, 132.5, 132.4, 127.9, 122.8, 117.1, 115.9, 95.3, 95.2, 56.1, 31.9, 30.0, 29.7–29.3, 28.7, 22.7, 14.1 ppm; IR (ATR): $\tilde{\nu}$=2912, 2848, 1513, 1469, 1433, 1306, 1251, 1225, 1202, 1151, 1126, 1075, 993, 921, 815, 765, 717 cm^{-1}; HRMS (ESI): m/z calcd for $C_{27}H_{46}O_4Na$: 457.3288 [M+Na]$^+$; found 457.3293. (*E*)-**4**: ^{1}H NMR (250 MHz, $CDCl_3$): δ=7.17 (d, J=2.5 Hz, 1H), 7.08 (d, J=7.5 Hz, 1H), 6.93 (dd, J=7.5, 2.5 Hz, 1H), 6.30 (d, J=16.3 Hz, 1H), 6.10 (dt, J=16.3, 7.5 Hz, 1H), 5.26 (s, 2H), 5.20 (s, 2H), 3.54 (s, 3H), 3.50 (s, 3H), 2.18 (m, 2H), 1.40 (m, 2H), 1.38–1.20 (m, 24H), 0.85 ppm (t, J=6.3 Hz, 3H); ^{13}C NMR (62.5 MHz, $CDCl_3$): δ=147.2, 146.0, 132.8, 130.0, 128.8, 120.0, 116.6, 113.8, 95.3, 56.0 32.8, 31.8, 29.5–29.0, 22.5, 13.9 ppm; IR (ATR): $\tilde{\nu}$=2915, 2847, 1510, 1465, 1430, 1257, 1223, 1206, 1149, 1123, 1073, 998, 957, 918, 861, 791, 764, 722 cm^{-1}.

1,2-Bis(methoxymethoxy)-4-heptadecylbenzene (5): A stirred solution of a mixture of (*Z*)- and (*E*)-**4** (1.55 g, 3.57 mmol) in EtOAc (37 mL) was hydrogenated over Pd/C (174 mg) under of H_2 (1 atm) for 5 h. The catalyst was removed by filtration over celite and the solvent was evaporated to afford **5** as a colorless oil (1.53 g, 98% yield). ^{1}H NMR (250 MHz, $CDCl_3$): δ=7.06 (d, J=8.3 Hz, 1H), 6.98 (d, J=2.0 Hz, 1H), 6.77 (dd, J=8.3, 2.0 Hz, 1H), 5.22 (s, 2H), 5.20 (s, 2H), 3.52 (s, 3H), 3.51 (s, 3H), 2.53 (t, J=7.5 Hz, 2H), 1.55 (m, 2H), 1.38–1.24 (m, 28H), 0.88 ppm (t, J=6.3 Hz, 3H); ^{13}C NMR (62.5 MHz, $CDCl_3$): δ=146.9, 145.0, 137.4, 122.0, 116.8, 116.7, 95.5, 95.3, 56.0, 55.9, 35.3, 31.8, 31.4, 29.5–29.2, 22.5, 13 ppm; IR (ATR): $\tilde{\nu}$=2917, 2849, 1515, 1468, 1244, 1203, 1149, 1129, 1074, 1002, 919, 858, 798, 764, 725, 677 cm^{-1}; HRMS (ESI+): m/z calcd for $C_{27}H_{48}O_4Na$: 459.3445 [M+Na]$^+$; found 459.3455.

4-Heptadecylcatechol (1): Compound **5** (1.10 g, 2.52 mmol) was dissolved in MeOH (50 mL) and 10 drops of concentrated HCl were added. The reaction mixture was heated to reflux for 2 h. After cooling, the solvent was evaporated under reduced pressure to yield a solid residue, which was dissolved in diethyl ether (15 mL) and washed with a saturated aqueous solution of $NaHCO_3$ (3× 5 mL). The organic phase was dried over $MgSO_4$ and concentrated under vacuum to provide **1** as a white solid (750 mg, 86%). ^{1}H NMR (250 MHz, $CDCl_3$): δ=6.77 (d, J=7.5 Hz, 1H), 6.71 (d, J=2.5 Hz, 1H), 6.61 (dd, J=7.5, 2.5 Hz, 1H), 2.49 (t, J=7.3 Hz, 2H), 1.55 (m, 2H), 1.35–1.20 (m, 28H), 0.87 ppm (t, J=6.5 Hz, 3H); ^{13}C NMR (62.5 MHz, C_3D_6O, $CDCl_3$): δ=145.6, 143.7, 135.2, 120.3, 116.2, 115.9, 35.9, 32.6, 30.7–30.0, 23.3, 14.3 ppm; IR (ATR): $\tilde{\nu}$=3344, 2915, 2848, 1520, 1470, 1443, 1356, 1282, 1264, 1254, 1183, 1115, 954, 868, 814, 790, 749, 717 cm^{-1}; HRMS (ESI+) m/z calcd for $C_{23}H_{40}O_2Na$: 371.2921 [M+Na]$^+$; found 371.2914.

STM investigation: General experimental procedures and STM data are included in the Supporting Information.

Theoretical calculations: We performed theoretical calculations of the thermodynamic free energy involved in the transfer of the different molecules of interest from liquid solution to the graphite surface. The calculations were made employing the MD approach, which is the technique of choice in liquid-phase simulations (instead of much simpler total-energy molecular-mechanics calculations). The MD method is based on the numerical solution of the Newton equations of motion for all atoms of a molecular system constrained to the thermodynamic conditions (*T*, *p*, and so forth). All the MD simulations were performed using the NAMD2 software,[15] version 2.7 running in parallel at the Finisterrae Supercomputer (CESGA Supercomputing Center, Spain). In our simulations, a typical production run contained about 2×10^4 atoms in the simulation box, and the equations of motion were solved with a time step of 2 fs. In all our simulations, the temperature was maintained constant (at 20, 45, or 80 °C) using the Langevin thermostat with a relaxation constant of 1 ps^{-1}. In simulations at constant pressure and temperature (NPT), we employed the Nosé-Hoover-Langevin piston as implemented in NAMD2 with an oscillation period of 100 fs and a decay time of 50 fs to adjust the solution pressure at 1 atm.

The model for the molecules was based on the CHARMM22/CMAP force field[16] designed for biomolecular simulations. The modular structure of this force field (constructed from quantum-chemical calculations of the interactions between model compounds and water) allows the model parameters for a given organic compound to be easily constructed from the basic building blocks of the force field. Within this force field, the intramolecular interactions contained bonding, torsion, and dihedral potentials; furthermore, intermolecular interactions were described by electrostatic interactions (modeled with partial charges) and a Lennard-Jones interaction potential. The values of all the partial charges and other relevant details of the force field are given in the Supporting Information to ensure reproducibility of our results. We should note that in this force field hydrogen bonds appear in a natural way as a result of the interaction between partial charges. Previous reports have shown the validity of this kind of force field for describing the role of hydrogen bonding in self-assembly at interfaces.[17]

The procedure employed in the simulations is the following: first, we conducted a NPT simulation of a system containing 400 nonanoic acid molecules and 14 4-heptadecylcatechol molecules inside a cubic box with periodic boundary conditions in all directions. The barostat was adjusted to 1 atm and the thermostat to 20, 45, or 80 °C. After a simulation run of 2.4 ns, the solution was considered to be equilibrated because all the magnitudes of interest (i.e., size of simulation box, pressure, and temperature) were clearly stabilized. The final configuration of the solution was placed in contact with a graphite surface of 32.65 nm^2, thus obtaining a starting configuration for further simulations. The graphite solid was made with 7500 atoms with a thickness of 6 atomic layers. To speed up our high time-consuming MD simulations, all the atoms of the graphite substrate were maintained fixed in their equilibrium positions, an approximation that is innocuous because we do not expect any reconstruction or chemical alteration of the graphite surface. A second set of MD simulations at constant temperature (NVT conditions) were run to allow reach equilibration of the solution with the surface and adsorption/desorption events. Periodic boundary conditions were also employed in all directions, thus employing a simulation cell [Å] with vectors (30.7, −53.175, 0), (30.7, 53.175, 0), and (0, 0, 110) . This cell follows the geometry of graphite in the *x* and *y* directions and allows for a large space above the solution in the *z* direction to avoid spurious image interactions. The configuration obtained after 10 ns of simulation at the three different temperatures was employed as the starting point for our production runs. Each nanosecond of the NVT simulations required to be run for around 0.2 days in 32 Itanium Montvale processors.

In our production runs, we computed the equilibrium free-energy profiles (potentials of the mean force), thus characterizing the thermodynamic process of the transfer of molecules from solution to the interface and vice versa (see the snapshots in Figure 2 for an illustration). These free-energy profiles were computed by using a new,[18] fast, and efficient adaptive biasing force (ABF) methodology implemented in version 2.7 of NAMD2. The reaction coordinate for the ABF calculation was the *z* coordinate of the center of mass of the molecule that was transferred. We performed six different simulation runs that corresponded to the determination of the free-energy profile for each molecule (i.e., compound **1** or nonanoic acid) at three different temperatures (20, 45, and 80 °C) with a resolution of 0.2 Å for the reaction coordinate. The force constant employed in the calculations was the default value of 10 kcal mol^{-1} $Å^2$, and the simulations were typically run for 10 ns. All the other parameters of the simulation were the same those employed in the previous NVT simulation. Each nanosecond of the MD-ABF simulations required to be run around for 1.57 days in 32 Itanium Montvale processors.

Also, for comparison with the thermodynamic calculations, we performed energy-minimization calculations for the same models of the molecules to compute the energy of molecules adsorbed at the graphite surface. Comparison of the obtained energy with free-energy calculations was employed to clarify the role of the thermodynamics of solution in the self-assembly of molecules at the surface.

Acknowledgements

This work was partly funded by grants MAT 2009–13977-C03, CTQ2007–60613/BQU, CTQ2010–15380/BQU, CONSOLIDER NANOSELECT-CSD2007–00041, and FIS2009–13370-C02–02. J.S.-P. thanks the Generalitat de Catalunya for a FI predoctoral grant and the Institut Català de Nanotecnologia for their support. We also acknowledge the CESGA Supercomputing Center for computational time at the Finisterrae Supercomputer and technical assistance.

[1] H. Lee, N. F. Scherer, P. B. Messersmith, *Proc. Natl. Acad. Sci. USA* **2006**, *103*, 12999–13003.
[2] M. J. Sever, J. T. Weisser, J. Monahan, S. Srinivasan, J. J. Wilker, *Angew. Chem.* **2004**, *116*, 454–456; *Angew. Chem. Int. Ed.* **2004**, *43*, 448–450.
[3] a) Y. Kuraku in *Urushi: Proceedings of the Urushi Study Group* (Eds.: N. S. Brommelle, P. Smith), Getty Conservation Institute, California, USA, **1988**, pp. 45–51; b) E. J. Kidder, *Ancient People and Places*, Thames and Hudson, Japan, **1959**.
[4] J. Kumanotani, *Prog. Org. Coat.* **1995**, *26*, 163–195.
[5] R. Lu, Y. Kamiya, T. Miyakoshi, *Talanta* **2006**, *70*, 370–376.
[6] a) Y. Lee, H. J. Cheng, S. Yeo, C.-H. Ahn, H. Lee, P. B. Messersmith, T. G. Park, *Soft Matter* **2010**, *6*, 977–983; b) S. A. Burke, M. Ritter-Jones, B. P. Lee, P. B. Messersmith, *Biomed. Mater.* **2007**, *2*, 203–210; c) H. Lee, B. P. Lee, P. B. Messersmith, *Nature* **2007**, *448*, 338–341; d) B. P. Lee, C.-Y. Chao, F. N. Nunalee, E. Motan, K. R. Shull, P. B. Messersmith, *Macromolecules* **2006**, *39*, 1740–1748; e) M. Yu, T. J. Deming, *Macromolecules* **1998**, *31*, 4739–4745.
[7] a) J. Xia, Y. Xu, J. Lin, *Prog. Org. Coat.* **2010**, *67*, 365–369; b) H. S. Kim, J. H. Yeum, S. W. Choi, J. Y. Lee, I. W. Cheong, *Prog. Org. Coat.* **2009**, *65*, 341–347; c) J. Xia, Y. Xu, B. Hu, J. Lin, *Prog. Org. Coat.* **2009**, *65*, 510–513; d) H. Lee, S. M. Dellatore, W. M. Miller, P. B. Messersmith, *Science* **2007**, *318*, 426–430.
[8] a) N. Henningsen, R. Rurali, C. Limbach, R. Drost, J. I. Pascual, K. J. Franke, *J. Phys. Chem. Lett.* **2011**, *2*, 55–61; b) W. Essolaani, F. Picaud, C. Ramseyer, P. Gambardella, M. Saïd, D. Spanjaard, M.-C. Desjonquères, *Surf. Sci.* **2011**, *605*, 917–922; c) A. Mugarza, N. Lorente, P. Ordejón, C. Krull, S. Stepanow, M.-L. Bocquet, J. Fraxedas, G. Ceballos, P. Gambardella, *Phys. Rev. Lett.* **2010**, *105*, 115702; d) S. Stepanow, J. Honolka, P. Gambardella, L. Vitali, N. Abdurakhmanova, T-C. Tseng, S. Rauschenbach, S. L. Tait, V. Sessi, S. Klyatskaya, M. Ruben, K. Kern, *J. Am. Chem. Soc.* **2010**, *132*, 11900–11901; e) U. Schlickum, F. Klappenberger, R. Decker, G. Zoppellaro, S. Klyatskaya, M. Ruben, K. Kern, H. Brune, J. V. Barth, *J. Phys. Chem. C* **2010**, *114*, 15602–15606; f) T. Suzuki, T. Lutz, D. Payer, N. Lin, S. L. Tait, G. Costantini, K. Kernae, *Phys. Chem. Chem. Phys.* **2009**, *11*, 6498–6504; g) J. Y. Park, Y. Qi, I. Ratera, M. Salmeron, *J. Chem. Phys.* **2008**, *128*, 234701; h) M. Tatarkhanov, E.

Fomin, M. Salmeron, K. Andersson, H. Ogasawara, L. G. M. Pettersson, A. Nilsson, J. I. Cerdá, *J. Chem. Phys.* **2008**, *129*, 154109; i) U. Schlickum, R. Decker, F. Klappenberger, G. Zoppellaro, S. Klyatskaya, W. Auwärter, S. Neppl, K. Kern, H. Brune, M. Ruben, J. V. Barth, *J. Am. Chem. Soc.* **2008**, *130*, 11778–11782; j) S. L. Tait, A. Langner, N. Lin, R. Chandrasekar, O. Fuhr, M. Ruben, K. Kern, *ChemPhysChem* **2008**, *9*, 2495–2499; k) F. Klappenberger, M. E. Cañas- Ventura, S. Clair, S. Pons, U. Schlickum, Z.-R. Qu, T. Strunskus, A. Comisso, C. Wöll, H. Brune, K. Kern, A. De Vita, M. Ruben, J. V. Barth, *ChemPhysChem* **2008**, *9*, 2522–2530; l) P. Cabrera-Sanfelix, D. Sánchez-Portal, A. Mugarza, T. K. Shimizu, M. Salmeron, A. Arnau, *Phys. Rev. B* **2007**, *76*, 205438; m) N. Lin, A. Langner, S. L. Tait, C. Rajadurai, M. Ruben, K. Kern, *Chem. Commun.* **2007**, 4860–4862; n) M. Ruben, D. Payer, A. Landa, A. Comisso, C. Gattinoni, N. Lin, J.-P. Collin, J.-P. Sauvage, A. De Vita, K. Kern, *J. Am. Chem. Soc.* **2006**, *128*, 15644–15651; o) N. Henningsen, K. J. Franke, I. F. Torrente, G. Schulze, B. Priewisch, K. Ruck-Braun, J. Dokić, T. Klamroth, P. Saalfrank, J. I. Pascual, *J. Phys. Chem. C* **2007**, *111*, 14843–14848; p) A. Dmitriev, H. Spillmann, S. Stepanow, T. Strunskus, C. Wöll, A. P. Seitsonen, M. Lingenfelder, N. Lin, J. V. Barth, K. Kern, *ChemPhysChem* **2006**, *7*, 2197–2204; q) E. Barrena, E. Palacios- Lidón, C. Munuera, X. Torrelles, S. Ferrer, U. Jonas, M. Salmeron, C. Ocal, *J. Am. Chem. Soc.* **2004**, *126*, 385–395; r) P. Gambardella, M. Blanc, H. Brune, K. Kuhnke, K. Kern, *Phys. Rev. B* **2000**, *61*, 2254.

[9] a) L.-M. Liu, S.-C. Li, H. Cheng, U. Diebold, A. Selloni, *J. Am. Chem. Soc.* **2011**, *133*, 7816–7823; b) S.-C. Li, L.-N. Chu, X.-Q. Gong, U. Diebold, *Science* **2010**, *328*, 882–884; c) S.-C. Li, J.-G. Wang, P. Jacobson, X.-Q. Gong, A. Selloni, U. Diebold, *J. Am. Chem. Soc.* **2009**, *131*, 980–984; d) M. Weinhold, S. Soubatch, R. Temirov, M. Rohlfing, B. Jastorff, F. S. Tautz, C. Doose, *J. Phys. Chem. B* **2006**, *110*, 23756–23769; e) G.-X. Wei, G.-B. Pan, L.-J. Wan, J.-C. Zhao, C.-L. Bai, *Surf. Sci.* **2002**, *520*, L625L632.

[10] a) J. Visser, N. Katsonis, J. Vicario, B. L. Feringa, *Langmuir* **2009**, *25*, 5980–5985; b) N. Katsonis, A. Marchenko, D. Fichou, N. Barrett, *Surf. Sci.* **2008**, *602*, 9–16; c) S. Lei, K. Tahara, F. C. De Schryver, M. Van der Auweraer, Y. Tobe, S. De Feyter, *Angew. Chem.* **2008**, *120*, 3006–3010; *Angew. Chem. Int. Ed.* **2008**, *47*, 2964–2968; d) N. Katsonis, E. Lacaze, B. L. Feringa, *J. Mater. Chem.* **2008**, *18*, 2065–2073; e) A. Nion, P. Jiang, A. Popoff, D. Fichou, *J. Am. Chem. Soc.* **2007**, *129*, 2450–2451; f) S. Furukawa, K. Tahara, F. C. De Schryver, M. Van der Auweraer, Y. Tobe, S. De Feyter, *Angew. Chem.* **2007**, *119*, 2889–2892; *Angew. Chem. Int. Ed.* **2007**, *46*, 2831–2834; g) N. Katsonis, J. Vicario, T. Kudernac, J. Visser, M. M. Pollard, B. L. Feringa, *J. Am. Chem. Soc.* **2006**, *128*, 15537–15541; h) M. Lackinger, S. Griessl, W. M. Heckl, M. Hietschold, G. W. Flynn, *Langmuir* **2005**, *21*, 4984–4988; i) M. M. S. Abdel-Mottaleb, N. Schuurmans, S. de Feyter, J. Van Esch, B. L. Feringa, F. C. de Schryver, *Chem. Commun.* **2002**, 1894–1895; j) A. Marchenko, N. Katsonis, D. Fichou, C. Aubert, M. Malacria, *J. Am. Chem. Soc.* **2002**, *124*, 9998–9999.

[11] a) A. Jefferson, M. V. Sargent, S. Wangchareontrakul, *Aust. J. Chem.* **1988**, *41*, 19–25; b) A. Groweiss, J. H. Cardellina II, L. K. Pannell, D. Uyakul, Y. Kashman, M. R. Boyd, *J. Nat. Prod.* **1997**, *60*, 116–121.

[12] a) X. Zhang, Q. Chen, G.-J. Deng, Q.-H. Fan, L.-J. Wan, *J. Phys. Chem. C* **2009**, *113*, 16193–16198; b) F. Tao, J. Goswami, S. L. Bernasek, *J. Phys. Chem. B* **2006**, *110*, 195662–19569.

[13] D. Rohde, C.-J. Yan, H.-J. Yan, L.-J. Wan, *Angew. Chem.* **2006**, *118*, 4100–4104; *Angew. Chem. Int. Ed.* **2006**, *45*, 3996–4000.

[14] M. Lang, W. Stelich, *Synthesis* **2005**, *6*, 1019–1027.

[15] J. C. Phillips, R. Braun, W. Wang, J. Gumbart, E. Tajkhorshid, E. Villa, C. Chipot, R. D. Skeel, L. Kale, K. Schulten, *J. Comput. Chem.* **2005**, *26*, 1781–1802.

[16] A. D. MacKerell Jr., M. Feig, C. L. III Brooks, *J. Comput. Chem.* **2004**, *25*, 1400–1415.

[17] C. D. Lorenz, J. Faraudo, A. Travesset, *Langmuir* **2008**, *24*, 1654–1658.

[18] J. Hénin, J. Fiorin, C. Chipot, M. L. Klein, *J. Chem. Theory Comput.* **2010**, *6*, 35–47.

Received: June 23, 2011
Revised: October 10, 2011
Published online: January 30, 2012

